JOURNAL OF GEOPHYSICAL RESEARCH, VOL. 112, A01102, doi:10.1029/2006JA011836, 2007

Wind/WAVES observations of high-frequency plasma waves in solar wind reconnection exhausts

K. E. J. Huttunen,[1] S. D. Bale,[2] T. D. Phan,[1] M. Davis,[1] and J. T. Gosling[3]

Received 8 May 2006; revised 29 September 2006; accepted 25 October 2006; published 18 January 2007.

[1] This paper studies high-frequency plasma waves during 28 encounters of the Wind spacecraft with solar wind reconnection exhausts. We use measurements by the Thermal Noise Receiver (TNR) and Time Domain Sampler (TDS) experiments on Wind/WAVES to survey characteristics of electron plasma waves and the most common regions where they are found. TNR spectrograms showed intense emission bursts ~4 kHz (corresponding to the ion acoustic range) during 79% of the events while around the local electron plasma frequency intense emission bursts were recorded for 39% of the events. The TDS instrument, operating at 120,000 samples per second, detected three kinds of electric waveforms: Langmuir waves, electron solitary waves (ESW), and wave packets with frequencies between ion and electron plasma frequencies typically interpreted as Doppler-shifted ion acoustic waves. Except for one very intense ESW event, the average amplitudes for all these three waveform types were similar, below 1 mV/m. We found an increased probability to observe intense plasma wave activity when the reconnection X-line region was approached. Wave activity may be present anywhere in the reconnection exhaust, although the boundary region of the exhaust appears to be the most dynamic region for wave activity. In particular, the majority of the captured ESW occurred near the exhaust boundaries.

Citation: Huttunen, K. E. J., S. D. Bale, T. D. Phan, M. Davis, and J. T. Gosling (2007), Wind/WAVES observations of high-frequency plasma waves in solar wind reconnection exhausts, *J. Geophys. Res.*, *112*, A01102, doi:10.1029/2006JA011836.

1. Introduction

[2] Magnetic reconnection plays a fundamental role in many astrophysical and space plasma phenomena by enabling a fast release of magnetic energy and a rapid topological rearrangement of magnetic field lines. While the occurrence of reconnection is well established [e.g., *Paschmann et al.*, 1979; *Sonnerup et al.*, 1981] the underlying microphysics is still poorly understood [e.g., *Sonnerup*, 1979; *Treumann*, 2001; *Vaivads et al.*, 2006], particularly the role of different plasma waves in the reconnection process. The ideal MHD condition can be broken by any terms in the generalized Ohm's law:

$$\mathbf{E} + \mathbf{V} \times \mathbf{B} = \frac{1}{ne}\mathbf{J} \times \mathbf{B} + \frac{1}{ne}\nabla \cdot \vec{P}_e + \frac{m_e}{ne^2}\frac{\partial \mathbf{J}}{\partial t} + \eta \mathbf{J}, \qquad (1)$$

where **E** and **B** are the electric and magnetic fields, **V** is the plasma bulk velocity, **J** is the electric current density, η is the resistivity, and n, m_e, and e are defined as usual. The first term on the right-hand side of equation (1) is the Hall effect associated with differential flow of ions and electrons, the second term is the electron pressure tensor ($\vec{P}_e$) term, and the third term the electron inertia term. In the case of a collisionless plasma resistivity η (final term of equation (1)) must arise from electron momentum changes through electron scattering from the wave electric fields generated by some microinstability [e.g., *Coroniti and Eviatar*, 1977]. This so-called anomalous resistivity as a mechanism to violate the frozen-in condition is supported by observations of strong plasma wave activity close to the reconnection X-line regions in the Earth's magnetosphere [e.g., *Coroniti and Eviatar*, 1977; *Bale et al.*, 2002; *Farrell et al.*, 2002; *Deng et al.*, 2004; *Vaivads et al.*, 2004] and in laboratory experiments [e.g., *Carter et al.*, 2002]. The wave modes observed in these studies include low-frequency waves such as lower hybrid waves as well as high-frequency waves such as ion acoustic, upper hybrid, and Langmuir waves. In addition, isolated bipolar electric field pulses called electron solitary waves (ESW) or electron holes have been frequently reported in association with magnetic reconnection events in the magnetotail [*Farrell et al.*, 2002; *Cattell et al.*, 2005] and at the magnetopause [*Cattell et al.*, 2002; *Matsumoto et al.*, 2003].

[3] Waves can also be important in terms of heating and accelerating electrons. Studies of solar flares have suggested that up to half of the energy released in the reconnection process is carried by energetic electrons [*Lin and Hudson*,

[1]Space Sciences Laboratory, University of California, Berkeley, California, USA.
[2]Department of Physics and Space Sciences, University of California, Berkeley, California, USA.
[3]Laboratory for Atmospheric and Space Physics, University of Colorado, Boulder, Colorado, USA.

0148-0227/07/2006JA011836$09.00

1971] and electrons accelerated to energies as high as 300 keV have been reported during magnetic reconnection in the distant magnetotail [*Oieroset et al.*, 2002]. Particularly, ESW and upper hybrid waves have been presented as possible candidates to cause large electron acceleration during the reconnection process [*Drake et al.*, 2003; *Farrell et al.*, 2003].

[4] The primary direct evidence of magnetic reconnection in space plasmas consists of observations of accelerated plasma jets emanating from the reconnection sites [e.g., *Paschmann et al.*, 1979; *Sonnerup et al.*, 1981; *Gosling et al.*, 1982; *Phan*, 2000]. Until recently, in situ studies of magnetic reconnection have been conducted only in the laboratory and in the Earth's magnetopause and magnetotail regions. Recently, clear signatures of magnetic reconnection have also been discovered in the solar wind [*Gosling et al.*, 2005a].

[5] In the solar wind reconnection exhausts convect antisunward with the solar wind flow and they exhibit characteristics of ''Petschek-type'' exhausts [*Petschek*, 1964; *Levy et al.*, 1964] with signatures of accelerated plasma flows away from the reconnection sites that are bounded by Alfvén or slow mode waves [*Gosling et al.*, 2005a, 2006a, 2006b; *Phan et al.*, 2006]. Typically, the transition from outside into the exhaust appears to be slow-mode-like and the estimated reconnection rates [*Phan et al.*, 2006; *Davis et al.*, 2006] are in the range of fast magnetic reconnection. Well over a hundred reconnection events in total have now been identified in the solar wind near 1 AU by Wind and ACE satellites [*Gosling et al.*, 2005a; *Phan et al.*, 2006; *Davis et al.*, 2006], at greater heliocentric distances and latitudes by the Ulysses satellite [*Gosling et al.*, 2006a], and also at heliocentric distances inward of 0.31 AU by Helios 1 and 2 [*Gosling et al.*, 2006b].

[6] The solar wind introduces an important new environment to investigate in detail the physical processes related to reconnection. Unlike patchy and random reconnection observed in the Earth's magnetosphere, in the solar wind the boundary conditions on the two sides of the current sheets are often stable and reconnection appears to be largely undriven and quasi-steady [*Phan et al.*, 2006]. We report in this paper the first observations of plasma wave activity in solar wind reconnection exhausts using observations from the WAVES experiment on the Wind satellite [*Bougeret et al.*, 1995]. WAVES records radio and plasma waves over a large range of frequencies and also provides the means to investigate in detail the waveforms in high time resolution. We analyze wave emissions around the local electron plasma frequency ($f_{pe} = \sqrt{n_o e^2/(4\pi^2 \epsilon_o m_e)}$, where n_o, e, ϵ_o, and m_e are defined as usual), and at frequencies between the ion and electron plasma frequencies. Note that the low-frequency plasma waves such as lower hybrid waves cannot be studied with WAVES detectors. The main objective of this paper is to investigate the occurrence rate and intensity of different plasma waves associated with solar wind reconnection events and to study the most common regions where these waves occur. Section 2 introduces the measurements used in this study, and in section 3 we provide an overview of the reconnection events. In section 4 we present an analysis of the wave emissions in different frequency domains, and in section 5 we look in detail at the captured waveforms. Finally, in section 6 we summarize and discuss the implications of our results.

2. Instrumentation

[7] The present analysis uses data from the Wind spacecraft that was launched in 1994 to monitor the solar wind upstream from the Earth and to investigate the Earth's magnetotail region with high time resolution. Solar wind plasma parameters are obtained from the 3-D Plasma (3DP) detectors [*Lin et al.*, 1995], while the magnetic field values are investigated using data from the Magnetic Field Instrument (MFI) [*Lepping et al.*, 1995]. Both MFI and 3DP measurements are given here as 3-s averages.

[8] Plasma wave activity is investigated using the Thermal Noise Receiver (TNR) and Time Domain Sampler (TDS) detectors included in the WAVES instrument. The spectral analyzer TNR measures electric spectral density covering the frequency range of 4 to 256 kHz. Data from the TNR receiver allow us to study emissions in two frequency domains relevant to reconnection physics: the frequency range covering the emissions between local ion ($f_{pi} = \sqrt{n_o e^2/(4\pi^2 \epsilon_o m_i)}$) and electron plasma frequencies and the emissions around the local electron plasma frequency.

[9] Activity around f_{pe} is commonly identified as Langmuir waves or upper hybrid waves. The upper hybrid frequency f_{uh} is calculated as $\sqrt{f_{pe}^2 + f_{ce}^2}$, where f_{ce} is the electron gyrofrequency ($f_{ce} = |e|B/2\pi m_e$). In the solar wind, f_{pe} is typically a few tens of kHz while f_{ce} is of the order of only about a few hundred Hz, making $f_{uh} \sim f_{pe}$. Langmuir waves and upper hybrid waves are distinguished by the polarization state: Langmuir waves propagate parallel to the ambient magnetic field while upper hybrid waves propagate obliquely [*Roth and Hudson*, 1986].

[10] Waves observed at $f_{pi} < f < f_{pe}$ are presumed to be ion acoustic waves at $f \sim f_{pi}$ that are Doppler-shifted by the motion of the solar wind [*Gurnett and Anderson*, 1977; *Gurnett and Frank*, 1978; *Mangeney et al.*, 1999]. For typical solar wind parameters near 1 AU the ion acoustic speed is much less than the solar wind speed and thus the frequency of the wave packet in the spacecraft frame is given almost entirely by the Doppler shift [*Gurnett and Frank*, 1978]: $f = (V_{sw}/\lambda) \times \cos \theta_{BV}$, where V_{sw} is the solar wind speed, λ is the wavelength of the wave, and θ_{BV} is the angle between the solar wind velocity and the magnetic field. *Gurnett and Frank* [1978] showed by studying plasma wave measurements on the Helios 1 and Helios 2 spacecraft that at 1 AU ion acoustic waves are observed at frequencies from about 1 to ~6.5 kHz. Thus for some events studied here the Doppler effect may not be enough to shift the frequency of the ion acoustic wave packet into the TNR range.

[11] TNR does not have the spectral resolution needed to resolve the details of the observed waves, but electric waveforms can be investigated using data obtained from the Time Domain Sampler (TDS) instrument, which is also a part of the WAVES experiment. TDS samples electric

Table 1. Selected Solar Wind Reconnection Exhausts Observed By Wind[a]

N_E	Date	Start Time	T_{ex} (s)	n	λ_M/λ_N	B_{shear}	$\|\Delta\mathbf{V}\|$, km/s	$\|\Delta V_A\|$	$\|\Delta Np\|$	ΔTp
1	11/16/97	1642:50	220	(0.84,0.38,−0.38)	2.1	152°	(15,4,10)	38	93%	39%
2	04/17/98	0054:34	198	(0.53,0.65,0.54)	15.9	109°	(25,22,1)	30	53%	175%
3	06/17/98	2309:00	79	(0.31,−0.20,0.93)	10.2	124°	(28,6,1)	4	3%	10%
4	08/21/98	2020:36	240	(0.88,−0.11,0.45)	8.3	147°	(16,12,6)	28	67%	119%
5	08/27/98	0536:11	49	(0.86,−0.38,0.33)	20.3	126°	(29,66,10)	63	73%	2%
6	09/17/98	0333:15	109	(0.93,0.32,−0.20)	8.0	154°	(27,21,4)	17	37%	88%
7	02/18/99	1026:24	281	(0.82,−0.57,0.06)	2.7	104°	(90,108,8)	104	222%	59%
8	06/15/99	1432:35	108	(0.81,0.16,−0.56)	18.9	167°	(2,23,2)	11	36%	90%
9	06/26/99	0546:00	550	(0.90,0.29,−0.32)	7.8	161°	(11,26,8)	8	16%	51%
10	07/22/99	0145:45	40	(0.40,0.64,−0.65)	57.7	109°	(71,2,5)	2	7%	37%
11	07/28/99	0435:59	189	(0.50,0.79,0.35)	4.9	95°	(0,24,2)	10	6%	23%
12	08/10/99	1838:20	356	(0.80,−0.60,0.1)	19.2	160°	(14,13,2)	7	10%	23%
13	09/19/99	0910:04	266	(0.84,0.36,0.41)	2.2	96°	(7,41,4)	20	25%	52%
14	04/19/00	0359:16	194	(0.72,0.48,−0.51)	4.8	154°	(21,2,2)	1	5%	2%
15	06/17/01	1630:23	157	(0.72,0.69,0.10)	20.4	147°	(40,6,1)	6	5%	26%
16	11/01/01	1758:25	93	(0.97,0.36,−0.52)	5.2	94°	(10,14,3)	28	41%	69%
17	02/02/02	0357:25	260	(0.68,0.67,−0.30)	5.1	140°	(15,21,3)	16	23%	52%
18	04/20/02	0041:30	300	(0.95,0.30,0.13)	3.9	170°	(75,37,9)	131	64%	51%
19	06/28/02	1526:32	333	(0.79,0.36,−0.50)	9.8	92°	(6,11,1)	4	20%	25%
20	03/02/03	2109:55	107	(0.97,0.24,−0.08)	15.7	134°	(20,1,3)	2	5%	21%
21	07/24/04	1151:10	235	(0.63,0.78,−0.03)	7.7	116°	(32,17,2)	183	65%	32%
22	08/26/04	0922:50	175	(0.54,0.60,0.58)	11.9	136°	(13,8,4)	4	17%	7%
23	09/14/04	2126:51	121	(0.50,0.25,−0.83)	23.7	140°	(41,40,2)	11	13%	5%
24	09/19/04	0641:00	670	(0.82,0.53,−0.22)	9.2	117°	(2,20,1)	16	43%	17%
25	10/08/04	0705:45	130	(0.81,0.19,0.56)	23.1	139°	(8,7,1)	2	3%	2%
26	10/11/04	1523:42	134	(0.64,0.77,0.07)	10.6	175°	(1,5,4)	10	0%	27%
27	10/29/04	0245:31	119	(0.36,0.02,0.93)	6.8	144°	(3,2,1)	1	8%	4%
28	12/06/04	0220:56	115	(0.53,0.75,0.40)	23.5	123°	(4,1,3)	11	19%	6%

[a]Columns give the event number (N_E), the event date and the start time, duration of the exhaust (T_{ex}), exhaust normal direction (**n**) in GSE, ratio of the intermediate eigenvalue (λ_M) to the minimum eigenvalue (λ_N), the magnetic field shear across the exhaust (B_{shear}), the differences in components of the velocity in LMN-coordinates ($\Delta\mathbf{V}$) and in the Alfvén speed (ΔV_A) across the exhaust, and finally the percentage changes in proton density ($|\Delta Np|$) and temperature ($|\Delta Tp|$) from the upstream to the downstream of the exhaust.

waveforms at rates up 120,000 samples/second on two orthogonal antennas, X and Y, whose physical lengths are 100 and 15 m, respectively. An event is a time series of 2048 data points and the duration of the event with the sampling rate 120,000 samples/second is 17 ms. Events above a hardware threshold (∼0.1 mV) are assigned a ''quality'' factor based on peak amplitude and added to a buffer. The buffer is then sorted and the lowest quality event drops off the end. Events are moved from the buffer to the telemetry stream as data rate and allocation allow. The typical event rate is order 100 events/day. As a result, if the spacecraft passes through a region of intense wave activity, the buffer will fill and a subsequent region with weaker waves will not be telemetered to the ground. This is often observed near the Earth's bow shock where upstream Langmuir waves overwhelm the buffer and no events from the shock itself are telemetered. An ''honesty'' channel telemeters events that are not selected for quality. Again, event rate depends on the telemetry mode. For further information on the TDS instrument, see *Bougeret et al.* [1995].

[12] In addition to electrons streaming upstream from the bow shock [*Filbert and Kellogg*, 1979; *Bale et al.*, 1997], the processes that cause intense plasma waves in the solar wind include electrons accelerated at interplanetary shocks [*Cane et al.*, 1981; *Bale et al.*, 1999] and electron beams associated with type III radio bursts [*Bardwell and Goldman*, 1976]. Plasma waves associated with solar wind reconnection are much less intense than the waves generated by the above mentioned processes. As a consequence, the TDS waveform captures made during the solar wind reconnection exhausts were mainly chosen for telemetry by the ''honesty'' channel.

3. Overview of the Reconnection Events

[13] The period from November 1997 to December 2004 was systematically investigated day by day to identify solar wind reconnection events. We carefully excluded all the events that were magnetically connected to the Earth's bow shock. Twenty-eight reconnections exhausts included in this study are listed in Table 1. The columns show the event number (N_E), start date, and start time of the exhaust as well as various other parameters discussed below. The duration time of the exhaust (T_{ex}) given in column 4 of Table 1 is the time interval between the crossings of the edges of the exhaust (Figure 1).

[14] The overall exhaust orientation can be estimated by minimum variance analysis (MVA) [*Sonnerup and Cahill*, 1967] of the magnetic field vector across the entire exhaust. Thus the exhaust normals given in this work should be considered an average of the two current sheet normals that bound the exhaust. In the following, magnetic field and solar wind velocity measurements are presented in LMN coordinates, where N is along the exhaust normal (minimum variance direction), M along the X-line (intermediate variance direction), and finally L along the antiparallel magnetic field direction (maximum variance direction). *Zhang et al.* [2005] compared current sheet normals obtained by MVA and by using current sheet crossing timings from four Cluster spacecraft. They found that when the ratio of the intermediate eigenvalue (λ_M) to the mini-

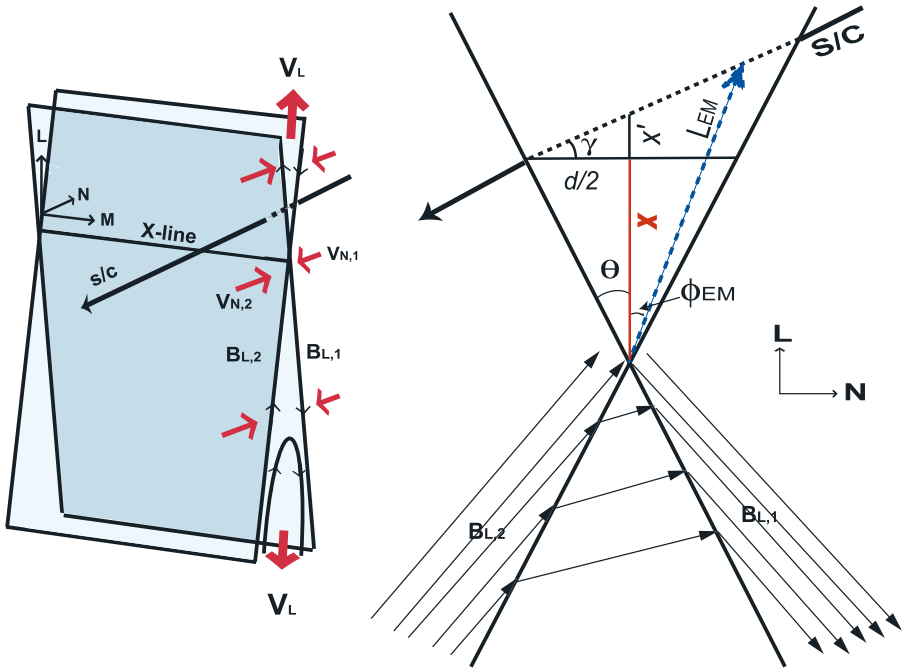

Figure 1. (a) Idealized schematic of the reconnection exhaust bounded by a pair of current sheets. Thin red arrows show the plasma inflowing to the exhaust (V_N) and thick red arrows denote the plasma jets accelerated away from the reconnection site (V_L). Reconnection occurs between magnetic field lines with large antiparallel components B_{L1} and B_{L2}. (b) Projection of a reconnection exhaust into the *NL*-plane. The black solid lines define boundaries of the reconnection exhaust (current sheets) where the magnetic field changes direction. The blue dashed arrow indicates a position of the emission along the spacecraft trajectory. The angle ϕ_{em} is measured relatively to the L-axis while L_{em} denotes the distance to the location of the emission burst from the X-line. Here θ is the wedge angle assumed to have a fixed value 0.03 rad in this study.

mum eigenvalue (λ_N) is large and the normal direction stationary the current sheet normal is well-defined. We required that the ratio λ_M/λ_N must have a value larger than 2.0 consistent with the study by *Lepping and Behannon* [1980]. The eigenvalue ratio λ_M/λ_N is given for each event in column 6 of Table 1. We also performed MVA on five sets of data intervals (1, 3, 5, 7, and 9 min) centered at the middle of each exhaust. The nested MVA yielded very consistent normal directions for different time intervals: The mean absolute deviations of longitudinal and latitudinal angles of the exhaust normals in GSE were typically only few degrees and were less than 8 degrees for all the events.

[15] General properties of the solar wind reconnection exhausts investigated here are consistent with those observed by previous studies: (1) The exhausts convect past a spacecraft on timescales of minutes indicating that they are relatively narrow on heliospheric scales in the direction of the exhaust normal [*Gosling et al.*, 2005a, 2006a, 2006b; *Phan et al.*, 2006]. The durations of the exhausts in our data set ranged between 40 s and ~11 min with the average duration of 192 ± 132 s. (2) The reconnection exhausts are typically embedded in a plasma characterized by low proton beta [*Gosling et al.*, 2005a, 2006a, 2006b; *Phan et al.*, 2006]. The average proton beta in the ambient solar wind for all events studied here was clearly less than unity ($\langle\beta\rangle_{ambient}$ = 0.38 ± 0.30) with only three events (26, 27, 28) embedded in the solar wind having the average proton beta >1. Within the exhausts the proton beta were enhanced with respect to the ambient value ($\langle\beta\rangle_{exhaust}$ = 1.93 ± 4.1). (3) In the solar wind reconnection may occur both as antiparallel reconnection and as component reconnection [*Gosling et al.*, 2006a, 2006b; *Davis et al.*, 2006]. Consistent with the results of the above-mentioned studies, we observed relatively large shears in the magnetic field ranging between 92° to 175° (column 7 in Table 1) with the average shear $\langle B_{shear}\rangle$ = 131° ± 23°. (4) The overall transitions from the outside into the exhausts are typically slow-mode on both sides characterized by increases proton density and temperature as well as decreases in magnetic field strength [*Gosling et al.*, 2005a, 2006a, 2006b; *Phan et al.*, 2006]. This was also a case for most of the events studied here except for three events (2, 5, and 16) that were associated with a density decrease on the other edge. The lack of density/temperature enhancements are possibly associated with the asymmetric plasma conditions on the opposite sides of the exhausts as suggested by *Gosling et al.* [2006b] the increases in density and temperature in the exhausts are likely a result of plasma interpenetration from opposite sides of the exhaust rather than from compression by slow mode shocks.

[16] In general, solar wind reconnection exhausts resemble more the accelerated flow events at the Earth's magnetopause than in the geomagnetic tail, as they are likely to occur between two quite distinct plasma states [*Gosling et al.*, 2005a, 2006b]. Many events in this study were associated with large differences in Alfvén speeds and in the

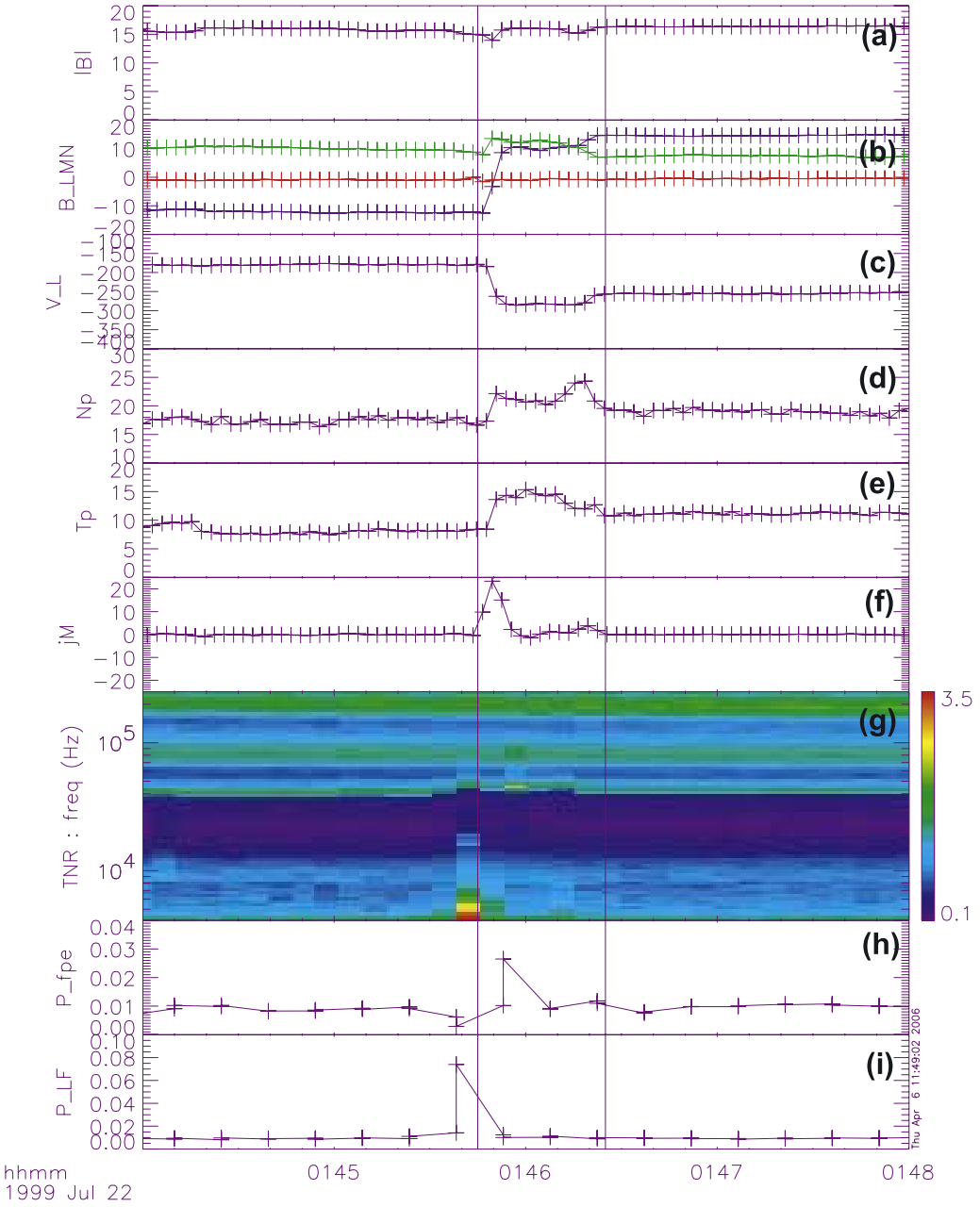

Figure 2. A 4 min time interval of the plasma and magnetic field measurements from Wind on 22 July 1999. From top to bottom are shown (a) magnetic field magnitude, (b) magnetic field components in LMN coordinates, (c) the plasma velocity L-component, (d) proton density, (e) proton temperature, (f) current density in the M-direction, (g) a TNR spectrogram, (h) electric field wave power (in μV/mHz) near the local electron plasma frequency, (i) and in the frequency band comprising the two lowest channels of TNR.

components of the velocity (columns 8 and 9 of Table 1) as well as in plasma density and temperature (columns 10 and 11 in Table) on the opposite sides of the exhausts.

[17] Figures 2 shows an example of a typical solar wind reconnection exhaust observed on 22 July 1999 (event 10). During this event, Wind was located in the free-streaming solar wind ~180 R_E upstream of the Earth close to the Sun-Earth line. In the center of the exhaust, plasma density and temperature are enhanced while magnetic field strength is slightly reduced with respect to the ambient values. The sign of the magnetic field L-component changed sharply at the front edge of the exhaust, maintained roughly a constant orientation in the center part of the exhaust, and finally B_L had a small but distinct rotation at the rear edge. In general (see also Figure 1b), two distinct magnetic field rotations are observed on the opposite edges of the exhausts, but the rotation can be considerably larger at the one edge than the other [*Gosling et al.*, 2005a, 2006a, 2006b]. The total magnetic field rotation across the exhaust was 114° and there was a very large guide field (B_M) associated with this events as well as a constant, nonzero normal component of the magnetic field of ~0.8 nT (B_N). There was also a clear

flow shear across the exhaust in V_L (74 km/s). Figure 2f gives the electric current along the M-direction:

$$j_M = \frac{1}{\mu_0}\frac{\partial B_L}{\partial N} \sim \frac{1}{\mu_0}\frac{\Delta B_L}{dtV_N} \quad (2)$$

where ΔB_L is the change in the magnetic field L-component, dt is the average time step, and V_N is the solar wind speed in the normal direction. Enhanced current densities are observed at the exhaust boundaries, particularly at the front boundary coinciding with the abrupt change in the magnetic field direction.

[18] To investigate enhancements in the plasma wave emission, we calculate the electric field wave power in the frequency band covering the two lowest channels of TNR (~4 kHz) and in a frequency band around the local electron plasma frequency (f_{pe} wave power). We refer to the emission near ~4 kHz by IA (Ion Acoustic) wave power as we believe that the emission at these frequencies present Doppler-shifted ion acoustic waves (see section 2). For the 22 July 1999 event the TNR spectrogram shows intense emission bursts at ~4 kHz and at the local f_{pe} at the front boundary of the exhaust (Figure 2g). The two lowest panels of Figure 2 show the associated sharp peaks in the f_{pe} wave power (Figure 2h) and in the IA wave power (Figure 2i), indicating the presence of Langmuir/upper hybrid waves and ion acoustic waves, respectively.

[19] Strong evidence that solar wind reconnection exhausts are bounded by Alfvén waves comes from the observations of anticorrelated changes in **V** and **B** (parallel propagating Alfven wave) at the one edge of the exhaust and correlated changes in **V** and **B** (antiparallel propagating Alfvén wave) at the other edge [*Gosling et al.*, 2005a, 2006b, 2006c]. Figures 3a–3g show a closeup of magnetic field and proton velocity components in LMN coordinates for the 22 July 1999 event presented in Figures 2 and for the reconnection event on 17 September 1998 (event 6). For the latter event, see *Gosling et al.* [2005b] for discussion of ACE observations during this exhaust. It is clearly seen from Figure 3 that for both events the changes in **B** and **V** anticorrelate in the leading part of the exhaust and correlate in the trailing part of the exhaust (note that for the 22 July 1999 event the correlation/anticorrelation in confined very close to the exhaust boundaries).

[20] Overplotted crosses in Figures 3b, 3d, 3f, and 3g show the flow prediction based on the so-called Walen test for Alfvén waves [e.g., *Sonnerup et al.*, 1981; *Gosling et al.*, 2005a; *Phan et al.*, 2006]:

$$\mathbf{V_{walen}} = \mathbf{V_{ref}} \pm \sqrt{\frac{1-\alpha_{ref}}{\mu_0\rho_{ref}}}\left[\frac{\mathbf{B}\rho_{ref}}{\rho} - \mathbf{B}_{ref}\right] \quad (3)$$

Here ρ is the plasma density, and α is the pressure anisotropy factor given by

$$\alpha = \left(p_{\parallel} - p_{\perp}\right)\mu_0 B^2, \quad (4)$$

where $p_{\parallel}$ and $p_{\perp}$ are the plasma pressures parallel and perpendicular to the magnetic field. The subscripts "ref" in equations (3) and (4) refer to the reference values of velocity and magnetic field measured upstream and downstream of the exhaust. The solid lines in Figure 3 denote the reference times at the leading and trailing edges of the exhaust used to calculate V_{ref}, B_{ref}, and α_{ref}. The leading and trailing predictions merge at 0146:16 UT for the 22 July 1999 event and at 0334:24 UT for the 17 September 1998 event. It is seen from the Figure 3 that there is a very good agreement between the predicted and observed flow both in magnitude and the components of the velocity.

[21] To compare plasma wave activity between the different events, it would be desirable to know the relative spacecraft distance from the X-line, L_X (see Figure 1b), that assuming a small wedge angle θ, can be approximated as

$$L_X = x + x' \approx \frac{d}{2}(\theta + \gamma), \quad (5)$$

where $d = V_N \times T_{ex}$ is the cross-section width of the exhaust in the direction of the exhaust normal and γ is the angle that the spacecraft trajectory makes with the N-axis. Although the observations suggests that solar wind reconnection exhausts are "Petschek-like," the assumption of the Petschek model is not essential for the analysis in this study. The dimensionless reconnection rates is given in terms of the inflow Alfvén Mach number that can be expressed by the ratio of the B_N and magnetic field strength and thus approximately equals to the wedge angle in the simple two-dimensional (2-D) geometry shown in Figure 1b:

$$M_{Ai} = \Delta V_N/(2V_{Ai}) = |B_N|/|\mathbf{B}| \approx \theta. \quad (6)$$

Here V_{Ai} is the inflow Alfvén speed and ΔV_N the change in V_N across the exhaust. In reality the reconnection exhausts may exhibit more complex 3-D structure and reconnection at multiple X-lines. However, the events studied here were all observed by Wind and ACE satellites, implying that they are steady and relatively well-defined events.

[22] In principle the reconnection rate could be determined by measuring the normal components of the velocity or magnetic field, but the results can be very uncertain as these quantities are too small to be measured reliably. Any slight uncertainties in the exhaust normal determination would result in significant error in B_N and V_N. For this reason we use here a constant wedge angle 0.03 rad for all events consistent with the estimations by *Phan et al.* [2006] and by *Davis et al.* [2006] for two solar wind reconnection events. The reconnection rate of 0.03 is close to the reconnection rate of 0.1 obtained by simulations of fast collisionless reconnection [e.g., *Shay et al.*, 1999] and is in the range of fast reconnection.

4. Observations of Wave Activity

[23] In this section we examine wave activity associated with solar wind reconnection exhausts. Enhanced emissions in TNR spectrograms were associated with the majority of the investigated events. Figure 4 shows the IA (Ion Acoustic) wave power (blue) and the f_{pe} wave power (red) in the reconnection exhaust as well as in 15 min periods surrounding the exhaust during three events. For all three of these events there are strong intensifications in the wave power in the f_{pe} band and/or in the IA band within the exhaust.

[24] The intensity and frequency spectrum of quasi-thermal noise depends on plasma parameters, such as the

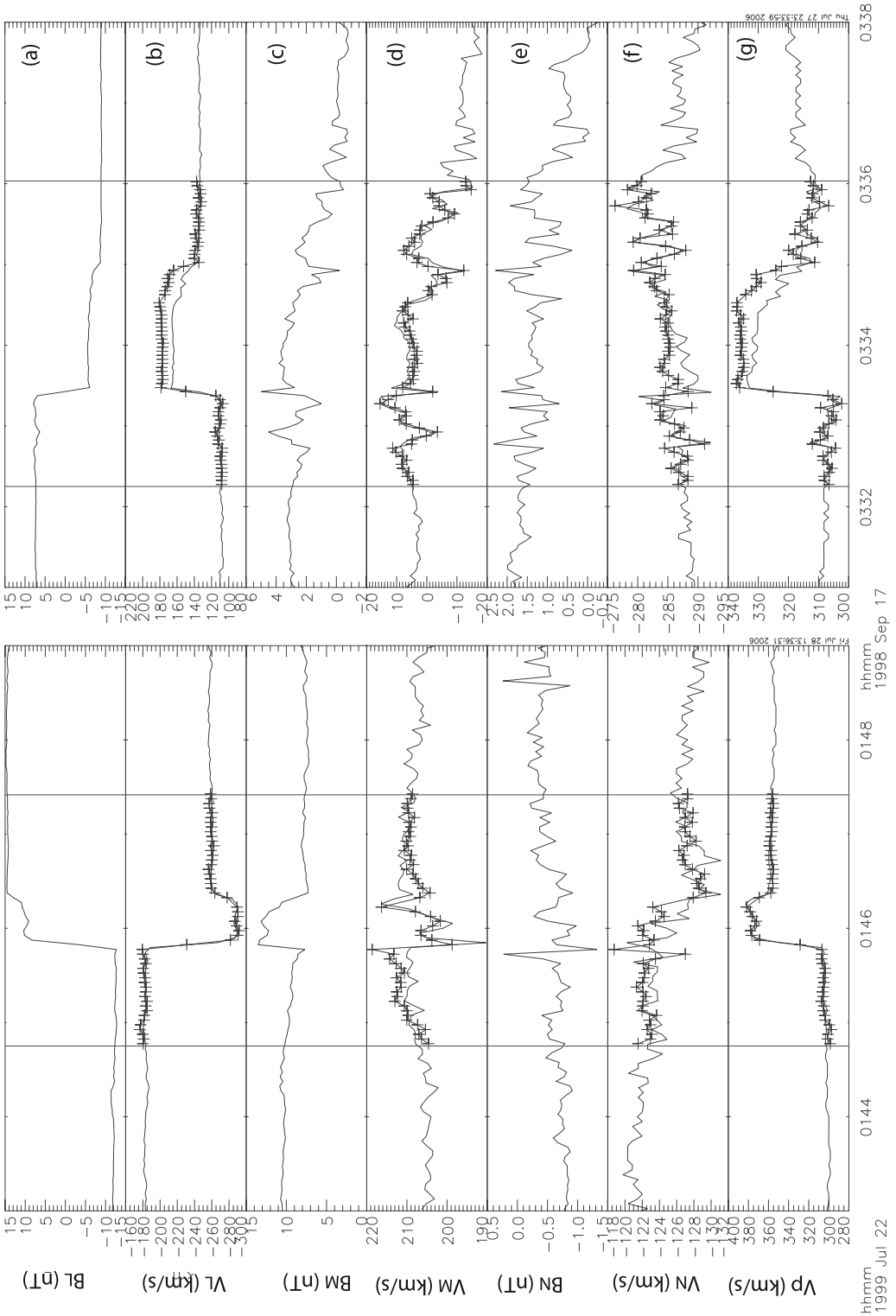

Figure 3. Magnetic field and proton flow velocity components and proton flow magnitude in LMN-coordinates for (left) the 22 July 1999 event and for (right) the 17 September 1998 events. (b, d, f, and g) The periods of overplotted crosses show the results of the Walen test (see text for details).

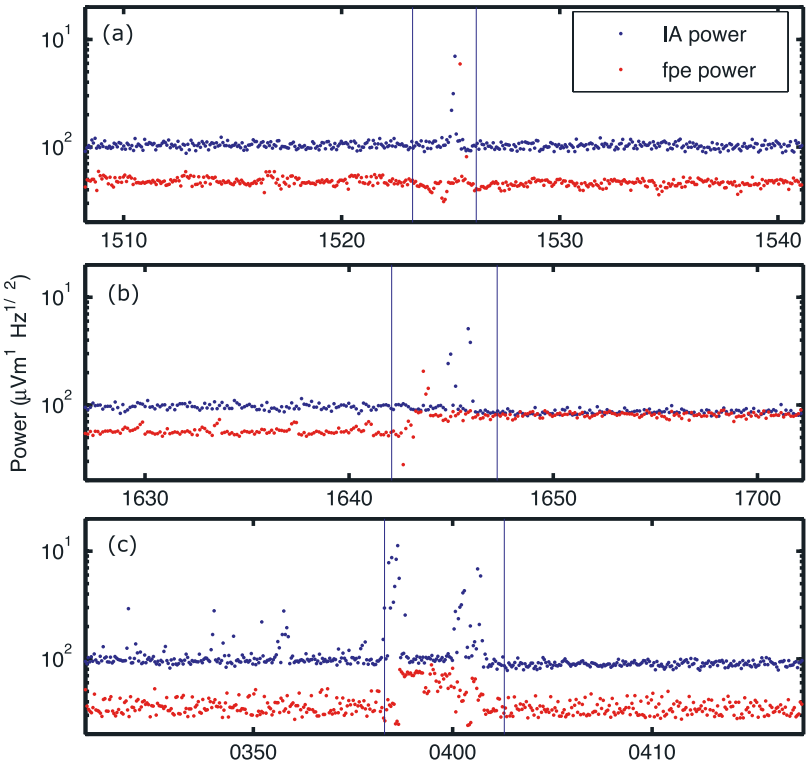

Figure 4. Electric field power in the two lowest channels of TNR (blue) and at the local f_{pe} (red) in the exhaust region and during 15 minutes time interval surrounding it for three investigated events: (a) 11 October 2004, (b) 16 November 1997, and (c) 2 February 2002. The reconnection exhaust is bounded by two solid lines in each panel.

temperature ratio of hot halo electrons and core electrons as well as their relative densities [*Meyer-Vernet and Perche*, 1989]. Investigated events took place under variable solar wind conditions and, as discussed in section 3 and shown by Table 1, many reconnection exhausts occurred at the interface between two quite different plasma states. As a consequence, the level of quasi-thermal noise varied considerably from event to event. For the 16 November 1997 event (Figure 4b) the level of quasi-thermal noise changed significantly across the exhaust, while for the 2 February 2002 event (Figure 4c) (see *Phan et al.* [2006] for more details of plasma and field measurements) there was a considerable change in the overall level of quasi-thermal noise within the exhaust region.

[25] To examine enhancements in the emission power with respect to the varying quasi-thermal noise level, we calculate the relative electric field wave power (P^{rel}) for each event. Wave power measured in a reconnection exhaust by TNR in 4.5 s intervals was divided by the average wave power for that particular exhaust. We defined the power in IA and f_{pe} emission to be significantly enhanced when P^{rel}_{IA} or P^{rel}_{fpe} were larger than 2.0. Enhancements in the IA wave power were twice as frequent as enhancements in the f_{pe} wave power: In 22 cases out of a total of 28 (79%) P^{rel}_{IA} was significantly enhanced while only in 11 cases out of total of 28 (39%) were associated with $P^{rel}_{fpe} > 2.0$.

[26] Figure 5 displays spacecraft trajectories projected in the *NL*-plane as well as calculated values of P^{rel}_{IA} and P^{rel}_{fpe} plotted along the trajectories. For clarity, only *L*-values up to 270 R_E are shown. Two thick solid lines correspond to exhaust boundaries. We have also calculated the relative power in a region of ambient solar wind comprising $0.2 \times T_{ex}$ for each event. Figure 5 demonstrates that intensifications in P^{rel}_{IA} and P^{rel}_{fpe} occur both around the exhaust boundaries as well as in the center of the reconnection exhausts. In addition, it is seen from Figure 5 that significant enhancements in P^{rel}_{IA} are considerably more frequent than significant enhancements in P^{rel}_{fpe}.

[27] In the following, we investigate the regions where the most intense emission bursts were observed. Figures 6a and 6b display calculated values of P^{rel}_{IA} and P^{rel}_{fpe} as a function of the distance from the X-line (L_{EM}) and Figures 6c and 6d as a function of the angle measured relatively to the L-axis ($|\phi_{EM}|$) for all 28 events. Definitions of L_{EM} and $|\phi_{EM}|$ are given in Figure 1b. Dashed lines in Figure 6 correspond to the boundaries of the exhausts (i.e., $|\phi_{EM}| = 0.03$). To emphasize the regions of the strongest emissions, histograms in Figure 7 show the occurrence rates for significantly enhanced relative wave power with respect to L_{EM} (left) and $|\phi_{EM}|$ (right) in 100 R_E and 0.006 rad bins, respectively. As the total number of all TNR measurements in each bin varies, we have calculated the occurrence rate using a percentage occurrence of significantly enhanced relative wave power observed in each L_{EM}- and $|\phi_{EM}|$-bin:

$$\text{Occurrence rate} = \frac{\text{Percentage of counts } P^{rel} > 2.0 \text{ in the bin}}{\text{Percentage of counts } P^{rel} > 2.0 \text{ for all bins}} \quad (7)$$

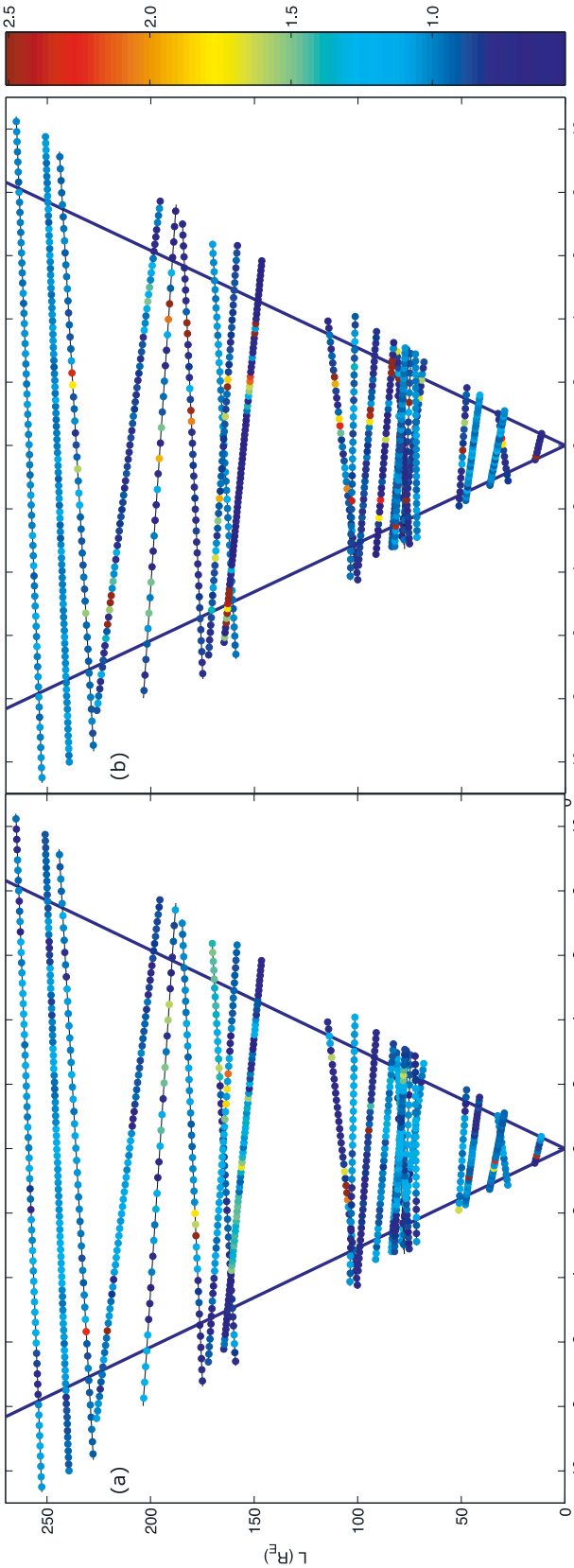

Figure 5. Wind trajectories plotted in the NL-plane. Calculated values of (a) P_{fpe}^{rel} and (b) P_{IA}^{rel} are shown as small dots along each trajectory. Dark blue dots corresponds to low values ($P_{rel} < 0.5$) and dark red corresponds to highest values ($P_{rel} > 2.5$).

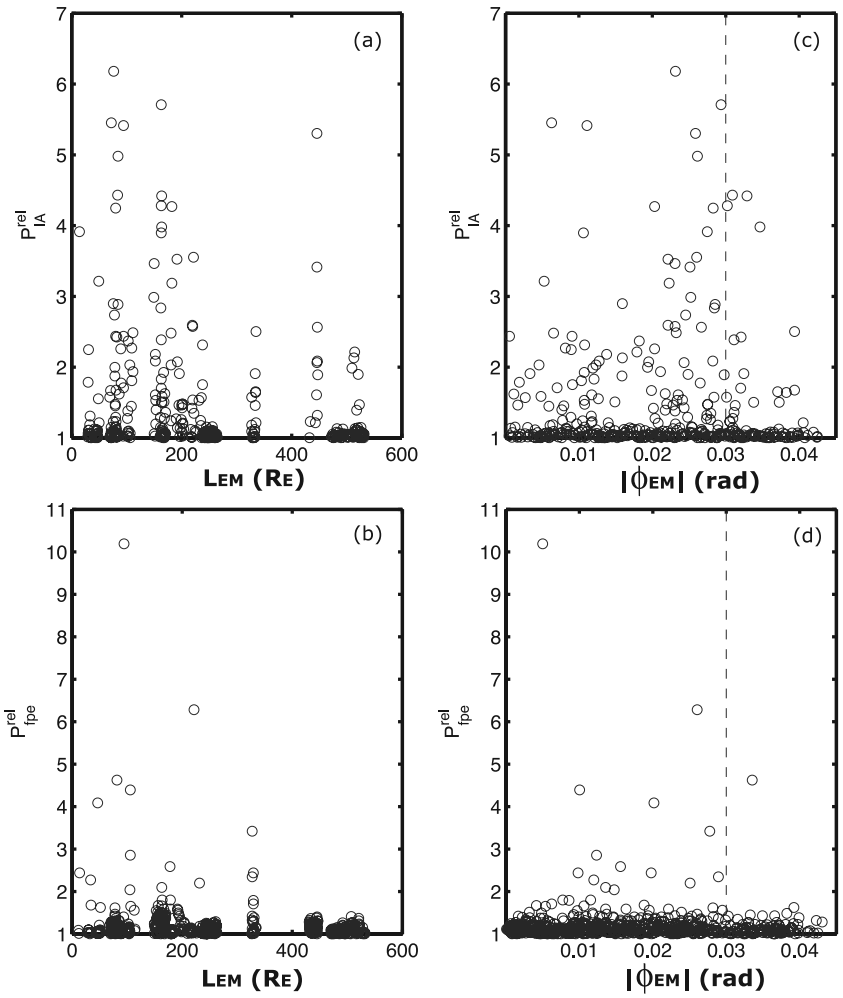

Figure 6. Relative IA wave power as a function of (a) L_{EM} and as a function of (c) $|\phi_{EM}|$. Relative f_{pe} wave power as a function of (b) L_{EM} and as a function of (d) $|\phi_{EM}|$. Here $|\phi_{EM}| = 0.03$ rad defines the boundaries of the exhaust.

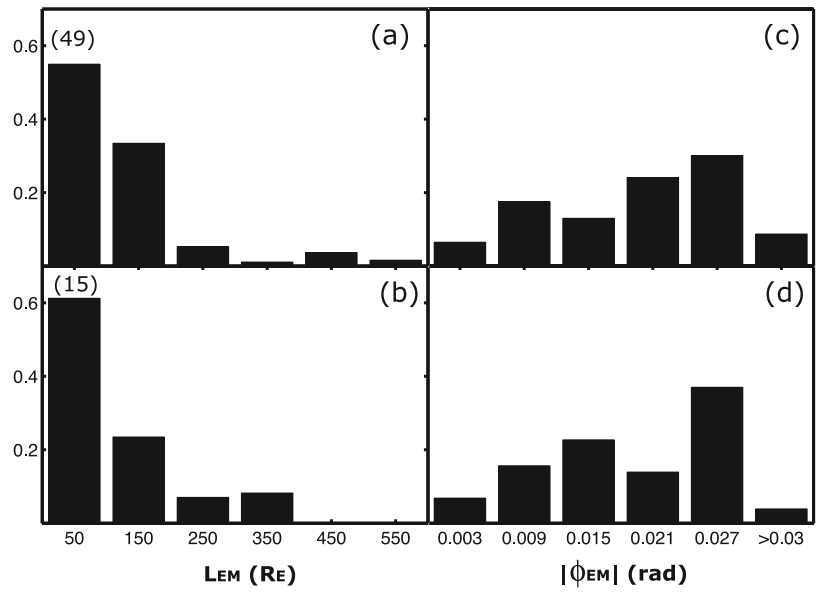

Figure 7. The percentage occurrence rate of $P^{rel} > 2.0$ in 100 R_E and 0.006 rad bins for (a and c) IA emission and (b and d) for f_{pe} emission.

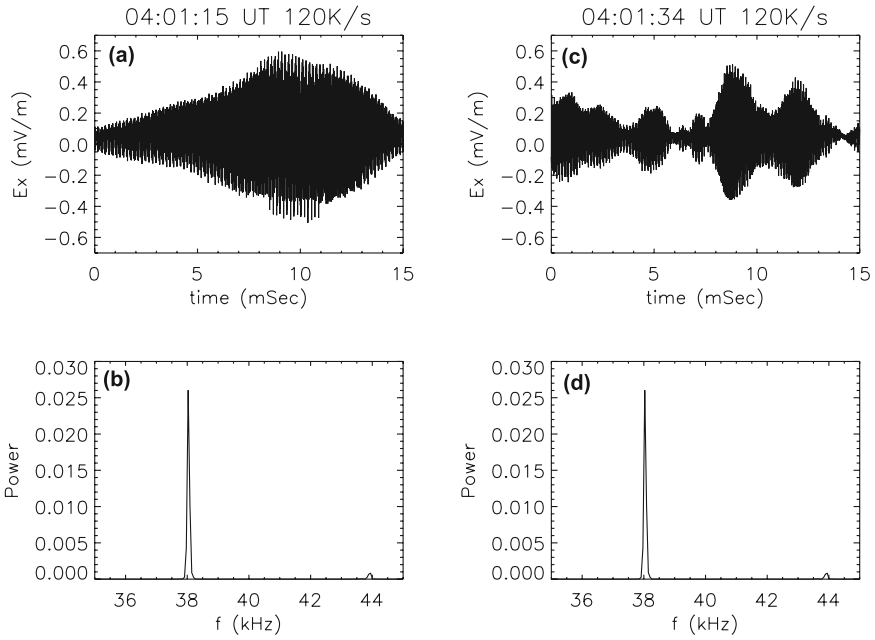

Figure 8. Waveforms observed by the TDS receiver during the 19 April 2000 reconnection event. (a) and (c) The electric field measured at the terminals of the x-antenna and (b) and (d) the corresponding power spectra.

Figures 6 and 7 illustrate that emissions bursts at ion acoustic frequencies and at the local f_{pe} are clearly more common and somewhat more intense the closer to the X-line the spacecraft crosses the exhaust. The distribution of the f_{pe} emission bursts (Figure 7d) peaks in the bin 0.027 rad. However, the bars showing intense f_{pe} emission bursts contain only 15 data points, so the associated errors may be very large. Overall the intense emission bursts at the IA range occur throughout the exhausts although the histograms of Figure 7c show that again the wave activity peaks in the 0.027 rad bin (0.023 rad $< \phi_{EM} <$ 0.03 rad) that represents the region adjacent to the exhaust boundary. The probability to observe intense emission bursts is lowest in the very center of the exhaust (i.e., in the 0.003 rad bin).

[28] As seen from Figure 4c, plasma wave activity is not unique for the reconnection exhausts in the solar wind. Several studies have shown that some plasma wave activity is frequently present in the solar wind even in the absence of significant perturbations [e.g., *Gurnett and Anderson*, 1977; *Gurnett and Frank*, 1978; *Mangeney et al.*, 1999]. To investigate the relationship between the wave activity in the reconnection exhausts and in the ambient solar wind, we calculate the rate of occurrences of the significantly enhanced emission bursts (i.e., $P^{rel}_{fpe} >$ 2.0 and $P^{rel}_{IA} > 2.0$) in the exhausts and in the surrounding solar wind 15 min before and after each exhaust. The rate of occurrence of significantly enhanced IA emissions was found to be ten times as high in the reconnection exhaust than in the ambient solar wind: $P^{rel}_{IA} > 2.0$ were observed at the rate of occurrence 4.5% in the exhaust and at 0.43% in the ambient solar wind. The significantly enhanced emissions at the local plasma frequency were also observed clearly more frequently in the exhaust than in the ambient solar wind, with the rate of occurrences of 2.4% and 0.1%, respectively.

5. TDS Waveforms

[29] TDS made waveform captures during 14 of the 28 events. Amplitudes of the waves observed in this study were small in an absolute sense and therefore all except one of the waveform captures were chosen for telemetry by the "honesty" channel (see section 2). Three types of electrostatic waves were detected in the center and around the boundaries of the reconnection exhausts, similar to those reported by *Mangeney et al.* [1999] in the free-streaming solar wind.

[30] Figures 8 and 9 show examples of the waveforms captured by TDS within the reconnection exhaust on 19 April 2000 and 2 February 2002 for a 120 k/s sampling rate. The electric field along the X-antenna is obtained by dividing the measured electric potential difference at the ends of the antenna by the effective length of the antenna (43.5 m). Waveforms in Figure 8 are high-frequency wave packets with amplitudes 0.63 mV/m and 0.54 mV/m. Polarization analysis (data not shown) showed that these waves are longitudinally polarized consistent with parallel propagating Langmuir waves. Figures 8b and 8d display power spectra for these waveforms from the X-antenna. The strongest signal for both waveforms is a peak near the local electron plasma frequency, 38.0 kHz and 37.5 kHz, respectively. The relative bandwidth is defined as $\Delta f/f_c$, where f_c is the central frequency and Δf the full width at half maximum of the profile. For the Langmuir waves in Figure 8 the relative bandwidths are small, 0.0056 and 0.0059, respectively. The bandwidth of the Langmuir waves may be used as a proxy for the width of the electron beam, which

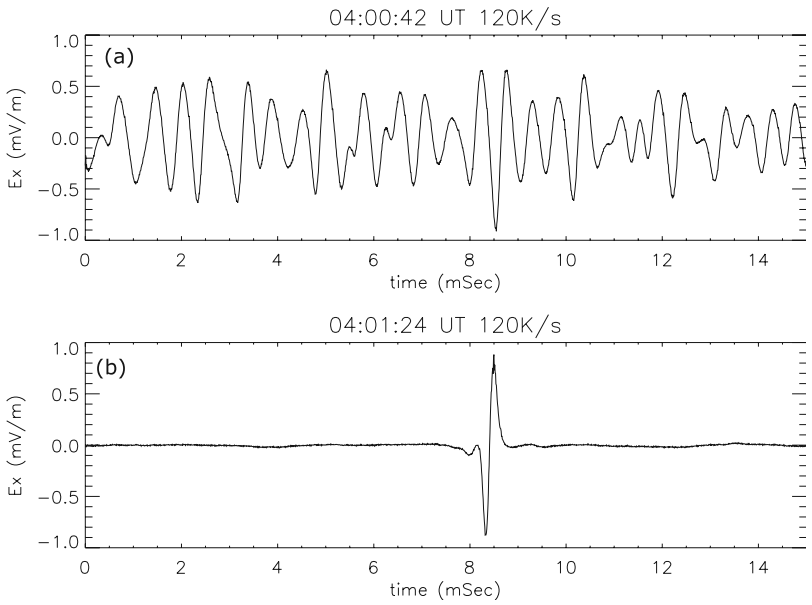

Figure 9. Waveforms observed by TDS during the 2 February 2002 reconnection event.

potentially can be compared with theories of electron acceleration in reconnection.

[31] Other types of waveforms we found associated with the reconnection events are illustrated in Figure 9. Figure 9a shows a typical low-frequency wave packet captured with a center frequency of 1.7 kHz and a peak amplitude of 0.7 mV/m. The waveform in Figure 9b is an example of a nonsinusoidal electron solitary wave (ESW) with an amplitude of 0.93 mV/m.

[32] The sampled low-frequency wave packets had center frequencies ranging between 0.54 and 4.6 kHz, consistent with the frequencies of ion acoustic waves observed by *Gurnett and Frank* [1978]. For two out of seven reconnection events that were not associated with IA emission bursts in TNR spectrograms, the TDS instrument made waveform captures of wave packets with center frequencies below 4 kHz. This suggests that for these events the Doppler effect was not sufficient to shift the frequency upwards into the TNR frequency range (see discussion in section 2).

[33] In the course of 14 events, TDS made 47 waveform captures, of which 17 were electron solitary waves, 17 were low-frequency wave packets, and 13 were Langmuir waves. Figures 10a and 10b show the maximum amplitudes of these waveforms as a function of L_{EM} and as a function of

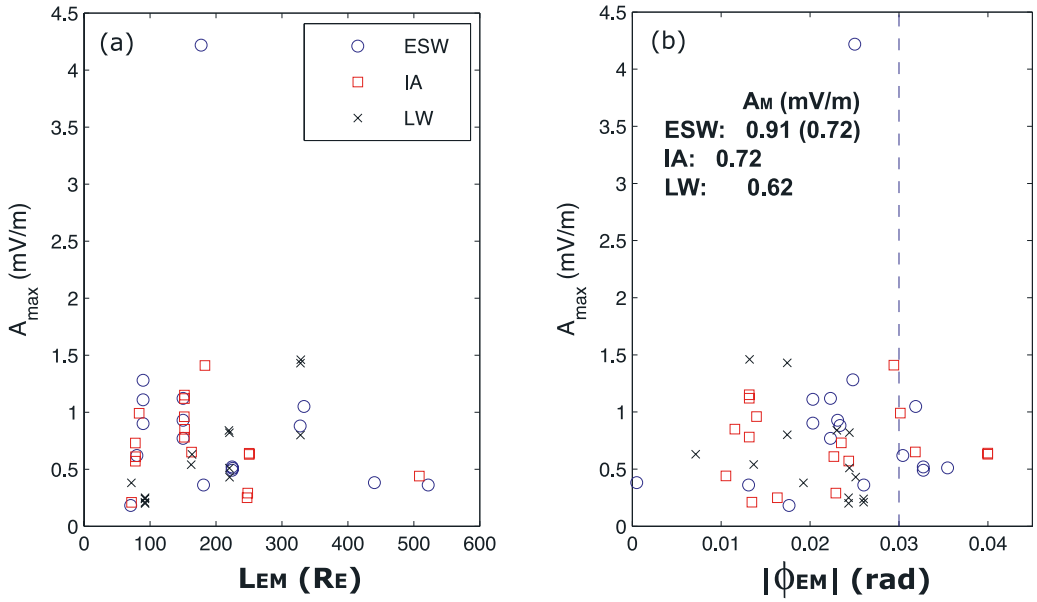

Figure 10. (a) Maximum amplitude of the waveforms observed by TDS as a function of L_{EM} and (b) as a function of $|\phi_{EM}|$. ESW is electron solitary wave; IA is ion acoustic wave; LW is Langmuir wave. Dashed line marks the exhaust boundary ($|\phi_{EM}|$ = 0.03 rad). On the right, values give the average amplitude for each waveform type. Number in parenthesis is the average amplitude for ESW when the highest amplitude event is excluded.

$|\phi_{EM}|$. There is no obvious correlation with either of these parameters. The average amplitudes for each wave type (given in Figure 10b) are very similar: 0.62 ± 0.39, 0.72 ± 0.31, and 0.92 ± 0.91 mV/m for Langmuir waves, ion acoustic waves, and ESW, respectively. Except for one very intense ESW sampled during a reconnection event on 16 November 1997 that had by far the largest amplitude in our survey (4.2 mV/m), the wave amplitudes were less than 1.5 mV/m.

[34] Figure 10b shows that all waveform types were sampled both near the exhaust boundaries as well as in the center of the exhaust, but the probability of a waveform capture increased when the boundary of the exhaust was approached. Particularly ESW events were clustered in the vicinity of the exhaust boundaries, whereas Langmuir waves and low-frequency waves were captured more randomly through the exhaust. In the very center region of the exhaust ($0 < \phi_{EM} \lesssim 0.01$ rad) only two waveform samples were obtained. In addition, Figures 6–7 demonstrate that in this region TNR recorded only a few emission bursts.

[35] *Mangeney et al.* [1999] studied TDS waveform samples in the solar wind during the 38-day interval from 20 May to 26 June 1995, when Wind was located more than 200 R_E from the Earth and thus for the most of the time was not magnetically connected to the Earth's bow shock. They found that ion acoustic waves, ESW, and Langmuir waves are a frequent feature in the solar wind. The *Mangeney et al.* [1999] study does not include the analysis of the possible solar wind perturbations causing the waves and thus it is hard to compare our results with theirs. The majority of the waves observed by *Mangeney et al.* [1999] are sampled in the ambient solar wind, but there is a small contribution from the waves generated by the electrons streaming from the bow shock and from the waves associated with significant solar wind perturbations such as stream interfaces [see *Mangeney et al.*, 1999, Figure 8]. The average amplitudes of the waves observed during the whole 38-day interval by *Mangeney et al.* [1999] were 0.22 ± 0.25, 0.19 ± 0.11, and 0.17 ± 0.12 mV/m for the Langmuir waves, ion acoustic waves, and ESW, respectively (C. Salem, private communication, 2006). These average amplitudes are somewhat lower than the average amplitudes of the waves observed in the solar wind reconnection exhausts (Figure 10b).

6. Discussion and Summary

[36] In this paper we have examined plasma wave activity during encounters with 28 solar wind reconnection exhausts using observations from the TNR and TDS experiments that are included in the WAVES instrument on the Wind spacecraft. These experiments allow the study of high-frequency plasma waves from about the local ion plasma frequency to the local electron plasma frequency in the solar wind. The lower-frequency plasma waves such as lower hybrid waves and whistler waves that are possibly also relevant for the reconnection process cannot be studied with these experiments.

[37] The general characteristics of exhausts observed in this study were consistent with previous studies of solar wind reconnection exhausts [*Gosling et al.*, 2005a, 2006a, 2006b; *Phan et al.*, 2006]. The average duration of the reconnection exhausts was about 3 min, a large fraction of them were embedded in low beta plasma (<1) and the exhausts were associated with relative large magnetic field shears across the exhausts with values ranging between 92° and 175°. Typically, but not always, the exhausts were associated with a slow-mode-like transition from the outside to inside the exhaust. Many events occurred at the interface of two quite different plasma states with large flow shears and large differences between Alfvén speeds as well as in densities and temperatures on the opposite sides of the exhausts.

[38] In order to compare the characteristics of the wave activity between the events, we needed to estimate the distance of the spacecraft to the X-line. We chose to use a fixed wedge angle (corresponding a constant dimensionless reconnection rate) for all the events because the determination of the wedge angle for the individual events can be very uncertain. The normal components of **B** and **V** are usually too small to be measured reliably and furthermore, the possible deviations from the assumed simple two-dimensional exhaust structure and the asymmetric nature of the reconnection process usually precludes the reliable determination of the wedge angle [see also *Gosling et al.*, 2006a]. In reality, the reconnection rate may vary from event to event; this can affect greatly the estimated spacecraft distances from the X-line. However, the statistical results of parametrization of the plasma wave intensity with distance from the exhaust boundaries (ϕ_{EM}) should be quite unaffected by possible differences in the reconnection rates between the events.

[39] Electric field wave power calculated from the TNR spectrograms were used to investigate wave activity in two frequency domains. The wave emissions observed at the lowest frequencies of TNR (~4 kHz) are likely to represent Doppler-shifted ion acoustic waves. We observed significant enhancements in this range for a large fraction of the events (79%). For the remaining events the Doppler shift may not have been sufficient to shift the frequency of the waves into the TNR range. In fact, for two of these events the TDS receiver made waveform samples of wave packets oscillating at frequencies just below the bottom of the TNR frequency range. Intense emission bursts at the local f_{pe} were less frequent than the ion acoustic bursts; only 39% of the investigated events were associated with significantly enhanced emission at the local f_{pe}.

[40] TDS waveform captures were available during 14 of 28 investigated reconnection events. Three different waveforms were identified: High-frequency wave packets oscillating near the local f_{pe}, ion acoustic wave packets with center frequencies ranging between 0.6 and 4.6 kHz and electron solitary waves. Polarization analysis indicated that high-frequency waves were longitudinally polarized, consistent with the Langmuir mode that propagates parallel to the ambient magnetic field. We found no obvious correlation between the wave amplitude and the distance from the X-line or the distance from the boundaries. With the exception of one very intense ESW with amplitude of 4.2 mV/m, all three types of waveforms had very similar average amplitudes, below 1 mV/m.

[41] The identified wave modes are similar to those associated with reconnection events in the Earth's magnetopause and magnetotail [*Farrell et al.*, 2002; *Matsumoto et al.*, 2003; *Deng et al.*, 2004; *Vaivads et al.*, 2004] as well as

those observed in the solar wind in the absence of significant perturbations [*Mangeney et al.*, 1999]. The amplitudes of the waves identified here were less intense than the amplitudes observed near the reconnection X-line regions in the Earth's magnetosphere, but somewhat higher than the amplitudes of electrostatic waves observed in the solar wind (C. Salem, private communication, 2006). We also found that intense emission bursts both at the ion acoustic range and near local plasma frequency to be clearly more common within the reconnection exhausts than in the ambient solar wind.

[42] We found an increased probability to observe intense wave emission close to the X-line, which suggests that the emissions are indeed associated with the reconnection process. In this study and in previous studies the vicinity of the X-line and exhaust boundaries have been recognized as the most dynamic regions in terms of plasma wave observations [e.g., *Drake et al.*, 2003; *Farrell et al.*, 2002; *Vaivads et al.*, 2004]. These are the regions where large density and temperature gradients, non-Maxwellian distribution functions and current-driven instabilities are likely to result various plasma waves which contribute to anomalous resistivity through wave-particle interactions and accelerate electrons to high energies [e.g., *Vaivads et al.*, 2006, and references therein]. Although in situ observations of plasma waves have been made only outside the diffusion region the magnetic field lines near the exhaust boundaries extend directly into the diffusion region. The exhaust boundary regions have been observed to extend and maintain their structure far away from the X-line region, at least up to hundreds of ion inertial lengths [e.g., *André et al.*, 2004].

[43] All three wave modes suggested by the observations in this study have interesting relations to reconnection microphysics. The turbulence associated with Langmuir waves will enhance anomalous resistivity, but it is questionable whether the resulting anomalous resistivity is sufficient to facilitate reconnection [e.g., *Treumann*, 2001]. However the observations of Langmuir/upper hybrid waves strongly suggests the presence of electron beams in the plasma, and therefore the distribution of Langmuir/upper hybrid waves can probably be used as a proxy for location of the electron beams in the reconnection exhausts. In addition, Langmuir waves/upper hybrid waves can result to acceleration of secondary electron beams [e.g., *Treumann*, 2001; *Farrell et al.*, 2003]. In this study the emission at the local f_{pe} and TDS captures of Langmuir wave packets were observed throughout the whole exhaust regions.

[44] Electron solitary waves are generated by two-stream or current-driven instabilities [*Omura et al.*, 1996]. Hence ESW can be regarded as a proxy for the spatial occurrence of bistreaming electrons and plasma currents. Intense bipolar electric fields associated with ESW can lead to strong electron scattering that will contribute in creating anomalous resistivity and furthermore ESW can efficiently accelerate electrons to high energies [*Drake et al.*, 2003; *Matthaeus et al.*, 2003]. Three-dimensional particle simulations by *Drake et al.* [2003] revealed that ESW form near the X-line region and along the boundaries of the exhausts. This is consistent with the results of this study, as we found a strong concentration of the ESW waveforms at the edges of the exhausts.

[45] Recent Vlasov simulations have highlighted the importance of anomalous resistivity provided by the ion acoustic instability [*Watt et al.*, 2002; *Petkaki et al.*, 2006]. Unlike lower-hybrid waves and whistler waves that are suppressed in high beta regions, ion acoustic waves can exist also near the reconnection X-line region where the magnetic field is weak [e.g., *Carter et al.*, 2002]. Ion acoustic waves are generated by current driven instabilities or by a bistream electron instability [*Omura et al.*, 1996]. We identified ion acoustic waves throughout the exhaust although the activity at these frequencies was most strongly concentrated along the boundaries.

[46] Although reconnection sites exhibit strong plasma wave activity, the detailed relationship between plasma waves and electron beams as well as the interplay between different plasma waves is still far from understood [e.g., *Treumann*, 2001]. The source of energetic electron beams has remained one of the long-standing problems in reconnection physics. For example, fermi-like acceleration of electrons from multiple magnetic islands [*Drake et al.*, 2005] and the acceleration associated with magnetohydrodynamic turbulence [*Ambrosiano et al.*, 1988] have been suggested as possible sources of electron beams. It is interesting to note that *Gosling et al.* [2005c] found no evidence for significant increases in energetic electron or ion intensity during or near seven solar wind reconnection exhausts. This topic will be studied in more detail in the future by Wind/3DP experiment that has a "burst-mode" allowing a determination of 3-s three-dimensional particle distribution functions for thermal, suprathermal, and energetic electrons.

[47] Our statistical survey of 28 solar wind reconnection exhausts has revealed an association between the reconnection process in the solar wind and plasma wave activity at the ion acoustic range and near local electron plasma frequency. The probability of intense wave activity was found to be highest near the X-line and along the exhaust boundaries. Although we found that plasma waves occur much more frequently in reconnection exhausts than in the ambient solar wind the importance of the observed wave modes to the reconnection process requires further investigation. The study of the occurrence of electron beams and current signatures and their relation to the observed plasma waves will be carried out in the future. The boundary conditions for the reconnection current sheets in the solar wind may differ significantly from those in the magnetosphere, which is likely to affect such things as the reconnection rate and the effectiveness of particle acceleration.

[48] **Acknowledgments.** We thank R. Lepping for the Wind Magnetic Field Investigation data, R. P. Lin for the Wind 3D-plasma data, and M. L. Kaiser for the WAVES data. The WAVES instrument on Wind was built by teams at the University of Minnesota, the University of Iowa, and the Observatoire de Paris Meudon, with support of NASA/GSFC. We want to acknowledge Chadi Salem for helping in the polarization analysis of the waveforms. Work at the University of Colorado was supported by NASA grant NNG05G555G.

[49] Amitava Bhattacharjee thanks the reviewers for their assistance in evaluating this paper.

References

Ambrosiano, J., W. H. Matthaeus, M. L. Goldstein, and D. Plante (1988), Test particle acceleration in turbulent reconnecting magnetic fields, *J. Geophys. Res.*, *93*, 14,383.

André, M., A. Vaivads, S. C. Buchert, A. N. Fazakerley, and A. Lahiff (2004), Thin electron-scale layers at the magnetopause, *Geophys. Res. Lett.*, *31*, L03803, doi:10.1029/2003GL018137.

Bale, S. D., D. Burgess, P. J. Kellogg, K. Goetz, and S. J. Monson (1997), On the amplitude of intense Langmuir waves in the terrestrial electron foreshock, *J. Geophys. Res.*, *102*, 11,281.

Bale, S. D., M. J. Reiner, J.-L. Bougeret, M. L. Kaiser, S. Krucker, D. E. Larson, and R. P. Lin (1999), The source region of an interplanetary type II radio burst, *Geophys. Res. Lett.*, *26*, 1573.

Bale, S. D., F. S. Mozer, and T. Phan (2002), Observation of lower hybrid drift instability in the diffusion region at a reconnecting magnetopause, *Geophys. Res. Lett.*, *29*(24), 2180, doi:10.1029/2002GL016113.

Bardwell, S., and M. V. Goldman (1976), Three-dimensional Langmuir wave instabilities in type III solar radio bursts, *Astrophys. J.*, *209*, 912.

Bougeret, J.-L., et al. (1995), Waves: the radio and plasma wave investigation on the Wind, *Space Sci. Rev.*, *71*, 231.

Cane, H. V., R. G. Stone, J. Fainberg, R. T. Stewart, J.-L. Steinberg, and S. Hoang (1981), Radio evidence for shock acceleration of electrons in the solar corona, *Geophys. Res. Lett.*, *8*, 1285.

Carter, T. A., H. Ji, F. Trintchouk, M. Yamada, and R. M. Kulsrud (2002), Measurement of lower-hybrid drift turbulence in a reconnecting current sheet, *Phys. Rev. Lett.*, *88*, doi:10.1103/PhysRevLett.88.015001.

Cattell, C., J. Crumley, J. Dombeck, J. Wygant, and F. S. Mozer (2002), Polar observations of solitary waves at the Earth's magnetopause, *Geophys. Res. Lett.*, *29*(5), 1065, doi:10.1029/2001GL014046.

Cattell, C., J. Dombeck, J. Wygant, J. F. Drake, M. Swisdak, W. Keith, A. Fazakerley, M. André, E. Lucek, and A. Balogh (2005), Cluster observations of electron holes in association with magnetotail reconnection and comparison to simulations, *J. Geophys. Res.*, *110*, A01211, doi:10.1029/2004JA010519.

Coroniti, F. V., and A. Eviatar (1977), Magnetic field reconnection in a collisionless plasma, *Astrophys. J. Suppl. Ser.*, *33*, 189.

Davis, M. S., T. D. Phan, J. T. Gosling, and R. M. Skoug (2006), Detection of oppositely directed reconnection jets in a solar wind current sheet, *Geophys. Res. Lett.*, *33*, L19102, doi:10.1029/2006GL026735.

Deng, X. H., H. Matsumoto, H. Kojima, T. Mukai, R. R. Anderson, W. Baumjohann, and R. Nakamura (2004), Geotail encounter with reconnection diffusion region in the Earth's magnetotail: Evidence of multiple X lines collisionless reconnection?, *J. Geophys. Res.*, *109*, A05206, doi:10.1029/2003JA010031.

Drake, J. F., M. Swisdak, C. Cattell, M. A. Shay, B. N. Rogers, and A. Zeiler (2003), Formation of electron holes and particle energization during magnetic reconnection, *Science*, *299*, 873.

Drake, J. F., M. A. Shay, W. Thongthai, and M. Swisdak (2005), Production of energetic electrons during magnetic reconnection, *Phys. Rev. Lett.*, *94*, doi:0.1103/PhysRevLett.94.095001.

Farrell, W. M., M. D. Desch, M. L. Kaiser, and K. Goetz (2002), The dominance of plasma waves near a reconnection X-line region, *Geophys. Res. Lett.*, *29*(19), 1902, doi:10.1029/2002GL014662.

Farrell, W. M., M. D. Desch, K. W. Ogilvie, and M. L. Kaiser (2003), The role of upper hybrid waves in magnetic reconnection, *Geophys. Res. Lett.*, *30*(24), 2259, doi:10.1029/2003GL017549.

Filbert, P. C., and P. J. Kellogg (1979), Electrostatic noise at the plasma frequency beyond the Earth's bow shock, *J. Geophys. Res.*, *84*, 1369.

Golsing, J. T., J. R. Asbridge, S. J. Bame, W. C. Feldman, G. Paschmann, N. Sckopke, and C. T. Russell (1982), Evidence for quasi-stationary reconnection at the dayside magnetopause, *J. Geophys. Res.*, *87*, 2147.

Gosling, J. T., R. M. Skoug, D. J. McComas, and C. W. Smith (2005a), Direct evidence for magnetic reconnection in the solar wind near 1 AU, *J. Geophys. Res.*, *110*, A01107, doi:10.1029/2004JA010809.

Gosling, J. T., R. M. Skoug, D. J. McComas, and C. W. Smith (2005b), Magnetic disconnection from the Sun: Observations of a reconnection exhaust in the solar wind at the heliospheric current sheet, *Geophys. Res. Lett.*, *32*, L05105, doi:10.1029/2005GL022406.

Gosling, J. T., R. M. Skoug, D. K. Haggerty, and D. J. McComas (2005c), Absence of energetic particle effects associated with magnetic reconnection exhausts in the solar wind, *Geophys. Res. Lett.*, *32*, L14113, doi:10.1029/2005GL023357.

Gosling, J. T., S. Eriksson, R. M. Skoug, D. J. McComas, and R. J. Forsyth (2006a), Petschek-type reconnection exhausts in the solar wind well beyond 1 AU: Ulysses, *Astrophys. J.*, *644*, 613.

Gosling, J. T., S. Eriksson, and R. Schwenn (2006b), Petschek-type magnetic reconnection exhausts in the solar wind well inside 1 AU: Helios, *J. Geophys. Res.*, *111*, A10102, doi:10.1029/2006JA011863.

Gurnett, D. A., and R. R. Anderson (1977), Plasma wave electric fields in the solar wind: Initial results from Helios 1, *J. Geophys. Res.*, *82*, 632.

Gurnett, D. A., and L. A. Frank (1978), Ion acoustic waves in the solar wind, *J. Geophys. Res.*, *83*, 58.

Lepping, R. P., and K. W. Behannon (1980), Magnetic field directional discontinuities: Minimum variance errors, *J. Geophys. Res.*, *85*, 4695.

Lepping, R. P., et al. (1995), The Wind magnetic field, *Space Sci. Rev.*, *71*, 207.

Levy, R. H., H. E. Petschek, and G. L. Siscoe (1964), Aerodynamic aspects of the magnetospheric flow, *AIAA J.*, *2*, 2065.

Lin, R. P., and H. S. Hudson (1971), 10–100 keV electron acceleration and emission from solar flares, *Sol. Phys.*, *17*, 412.

Lin, R. P., et al. (1995), A three-dimensional (3-D) plasma and energetic particle experiment for the Wind spacecraft of the ISTP/GGS mission, *Space Sci. Rev.*, *71*, 125–153.

Mangeney, A., C. Salem, C. Lacombe, J.-L. Bougeret, C. Perche, R. Manning, P. J. Kellog, K. Goetz, S. J. Monson, and J.-M. Bosqued (1999), Wind observations of coherent electrostatic waves in the solar wind, *Ann. Geophys.*, *17*, 307.

Matsumoto, H., X. H. Deng, H. Kojima, and R. R. Anderson (2003), Observation of electrostatic solitary waves associated with reconnection on the dayside magnetopause boundary, *Geophys. Res. Lett.*, *30*(6), 1326, doi:10.1029/2002GL016319.

Matthaeus, W. H., G. Qin, J. W. Bieber, and G. P. Zank (2003), Nonlinear collisionless perpendicular diffusion of charged particles, *Astrophys. J.*, *590*, L53.

Meyer-Vernet, N., and C. Perche (1989), Tool kit for antennae and thermal noise near the plasma frequency, *J. Geophys. Res.*, *94*, 2045.

Oieroset, M., R. P. Lin, T. D. Phan, D. E. Larson, and S. D. Bale (2002), Evidence for electron acceleration up to 300 keV in the magnetic reconnection diffusion region of Earth's magnetotail, *Phys. Rev. Lett.*, *89*, 195001.

Omura, Y., H. Matsumoto, T. Miyake, and H. Kojima (1996), Electron beam instabilities as generation mechanism of electrostatic waves in the magnetotail, *J. Geophys. Res.*, *101*, 2685.

Paschmann, G., B. U. O. Sonnerup, I. Papamastorakis, N. Sckopke, G. Haerendel, S. J. Bame, J. R. Asbridge, J. T. Gosling, C. T. Russell, and R. C. Elphic (1979), Plasma acceleration at the Earth's magnetopause: Evidence for reconnection, *Nature*, *282*, 243.

Petkaki, P., M. P. Freeman, T. Kirk, C. E. J. Watt, and R. B. Horne (2006), Anomalous resistivity and the nonlinear evolution of the ion-acoustic instability, *J. Geophys. Res.*, *111*, A01205, doi:10.1029/2004JA010793.

Petschek, H. E. (1964), Magnetic annihilation, in *ASS-NASA Symposium on the Physics of Solar Flares*, *NASA Spec. Publ.*, *SP-50*, 425–439.

Phan, T. D. (2000), Extended magnetic reconnection at the Earth's magnetopause from detection of bi-directed jets, *Nature*, *404*, 848.

Phan, T. D., et al. (2006), In-situ detection of a magnetic reconnection region extending more than 390 Earth radii in the solar wind, *Nature*, *439*, 175.

Roth, I., and M. K. Hudson (1986), Simulations of electron beam excited modes in the high-altitude magnetosphere, *J. Geophys. Res.*, *91*, 8001.

Shay, M. A., J. F. Drake, B. N. Rogers, and R. E. Denton (1999), The scaling of collisionless, magnetic reconnection for large systems, *Geophys. Res. Lett.*, *26*, 2163.

Sonnerup, B. U.Ö., and L. J. Cahill Jr. (1967), Magnetopause structure and attitude from Explorer 12 observations, *J. Geophys. Res.*, *96*, 171.

Sonnerup, B. U. O. (1979), Magnetic field reconnection, in *Solar System Plasma Physics*, edited by C. F. Kennel, L. T. Lanzerotti, and E. N. Parker, vol. 3, pp. 45–108, Elsevier, New York.

Sonnerup, B. U. O., G. Paschmann, I. Papamastorakis, N. Sckopke, G. Haerendel, S. J. Bame, J. R. Asbridge, J. T. Gosling, and C. T. Russell (1981), Evidence for magnetic field reconnection at the Earth's magnetopause, *J. Geophys. Res.*, *86*, 10,049.

Treumann, R. A. (2001), Origin of resistivity in reconnection, *Earth Planet Space*, *53*, 453.

Vaivads, A., Y. Khotyaintsev, M. Andre, A. Retino, S. C. Buchert, B. N. Rogers, P. Decreau, G. Paschmann, and T. D. Phan (2004), Structure of the magnetic reconnection diffusion region from four-spacecraft observations, *Phys. Rev. Lett.*, *93*(10), doi:10.1103/PhysRevLett.93.105001.

Vaivads, A., Y. Khotyaintsev, M. Andre, and R. Treumann (2006), Plasma waves near reconnection sites, *Lecture Not. Phys.*, *687*, 251.

Watt, C. E. J., R. B. Horne, and M. P. Freeman (2002), Ion-acoustic resistivity in plasmas with similar ion and electron temperatures, *Geophys. Res. Lett.*, *29*(1), 1004, doi:10.1029/2001GL013451.

Zhang, T. I., L. Baumjohann, W. Nakamura, R. Volwerk, M. Runov, A. Voros, Z. Glassmeier, and A. Balogh (2005), Neutral sheet normal direction determination, *Adv. Space Res.*, *36*, 1940–1954.

S. D. Bale, Department of Physics and Space Sciences, University of California, Berkeley, CA 94720, USA.

M. Davis, K. E. J. Huttunen, and T. D. Phan, Space Sciences Laboratory, University of California, Berkeley, 7 Gauss Way, Berkeley, CA 94720, USA. (huttunen@ssl.berkeley.edu)

J. T. Gosling, Laboratory for Atmospheric and Space Physics, University of Colorado, Boulder, CO 80303, USA.